aoa_paper_v4

July 15, 2017

1 Age of air intercomparison of global chemistry transport models

1.0.1 Maarten Krol[1,2,3], Marco de Bruine[2], Huug Ouwersloot[4], Andrea Pozzer[4], Yi Yin[5,6], Frederic Chevallier[5], Philippe Bousquet[5], Prabir Patra[7], Dmitry Belikov[8], Shamil Maksyutov[9], Sandip Dhomse[10], Wuhu Feng[11], and Martyn Chipperfield[10]

[1] Meteorology and Air Quality, Wageningen University, the Netherlands

[2] Institute for Marine and Atmospheric Research, Utrecht University, the Netherlands

[3] Netherlands Institute for Space Research SRON, Utrecht, the Netherlands

[4] Max-Planck institute for Chemistry, Mainz, Germany

[5] Laboraroire de Sciences du Climat et de l'Environnement (LSCE), Gif sur Yvette, France

[6] now at Jet Propulsion Laboratory, Pasadena, California, USA

[7] Japan Agency for Marine-Earth Science and Technology (JAMSTEC), Yokohama City, Japan

[8] Hokkaido University, Sapporo, Hokkaido, Japan

[9] Center for Global Environmental Research, National Institute for Environmental Studies, Tsukuba, Ibaraki, Japan

[10] School of Earth and Environment, University of Leeds, United Kingdom

[11] National Centre for Atmospheric Science, University of Leeds, United Kingdom

Correspondance: maarten.krol@wur.nl

version: 3.0

1.1 Abstract

p.m.

1.2 1 Introduction

Global chemistry transport models (CTMs) are used to simulate the composition of the Earth' atmosphere. The atmospheric composition is determined by exchange processes at the Earth surface, transport processes within the atmosphere, and chemical and physcial conversion processes. For example, the atmospheric mixing ratio distribution of CH_4 is driven by natural and anthropogenic emisions at the Earth' surface, atmospheric transport, and removal that is primarily driven by the atmospheric oxidants OH, Cl, and O^1D. The estimated atmospheric lifetime of CH_4 is approximately 9 years (Prather et al., 2012) mainly due to oxidation within the troposphere. Although some CH_4 destruction occurs in the stratosphere as witnessed by the decaying mixing ratios with altitude, the slow atmospheric transport from the troposphere to the stratosphere limits its impact on the atmospheric lifetime of CH_4. Other atmospheric constituents have widely different budgets. SF_6, for instance, has purely anthopogenic sources, mostly on the Northern Hemisphere (NH), and is only broken down in the upper stratosphere, resulting in a very long atmospheric lifetime of more than a 1000 years (Kovács et al., 2017). In contrast, ^{222}Rn is of purely natural origin. It emenates from land surfaces and quickly decays radioactively with a half life of 3.8 days.

Comparing results of CTMs to atmospheric observations allows assessment of the model performance. Depending on the atmospheric compound, various aspects of atmospheric transport can be investigated. Jacob et al. (1997) used ^{222}Rn and other short-lived tracers to evaluate the convective and synoptic scale transport in CTMs. Since the early 1990s the TransCom project focused on non-reactive tropospheric species like SF_6 (Denning et al., 1999) and CO_2 (Law et al. 1996, 2008). A more recent TransCom model intercomparison focused on the ability of models to properly represent atmospheric transport of CH_4, focussing on vertical gradients in the stratosphere, average long-term trends, seasonal cycles, interannual variations (IAVs) and interhemispheric (IH) gradients. The study concluded that models that show faster IH exchange for SF_6, also exhibit smaller IH gradients in CH_4. The estimated IH exchange time, calculated based on a time-invariant SF_6 emission rate, remained relative constant over the period of the analysis (1996–2007). Interestingly, a recent study highlighted the importance of IH transport variations in explaining the CO_2 mixing ratio difference between Mauna Loa on the Northern Hemisphere (NH) and Cape Grim, Tasmania on the Southern Hemisphere (SH) (Francey and Frederiksen, 2016). Specifically, the 0.8 ppm step-like increase of this difference between 2009 and 2010 was attributed to the opening and closing of the upper-tropospheric equatorial westerly duct, with an open-duct pattern from July 2008 to June 2009 (fast IH exchange), followed by closed-duct conditions between from July 2009 to June 2010 (slow IH exchange). Confirming this mechanism, Pandey et al. (2017) found again faster IH transport of CH_4 during the strong La Niña in 2011 using the TM5 CTM. The IH transport time scale plays an important role in atmospheric inversion studies. In these studies atmospheric observations are used to infer surface flux magnitude and distribution. For a long-lived greenhouse gas like CH_4 fast IH transport implies that a larger fraction of the emissions will be attributed to the NH (Patra et al., 2011, 2014).

The efficiency of models to mix the planetary boundary and to vent emissions to the overlying free atmosphere has been studied using SF_6 and generally revealed too slow

mixing over mid-latitude continents (Peters et al., 2004; Gloor et al., 2007). Together with the convective parameterisation, this determines the rate by which emissions (e.g. SF_6 and ^{222}Rn) are mixed vertically and interhemispherically (Locatelli et al., 2015a).

Another transport time scale relevant for atmospheric composition studies is troposphere-stratosphere exchange, driven by the Brewer-Dobson circulation (Butchard, 2014). Depending on the greenhouse gas scenario, global chemistry-climate model projections predict an accelleration of this global mass circulation of tropospheric air through the stratosphere. Stratospheric age of air and its temporal trend have been determined from SF_6 measurements from the MIPAS satellite (Stiller et al., 2012). Using a suite of stratospheric observations, Fu et al. (2015) quantified the acceleration of the Brewer-Dobson circulation 2.1% per decade for 1980–2009. Other modelling and experimental studies revealed that the atmospheric composition of the tropopuase layer strongly depends on the mixing processes that occur on a wide range of spatio-temporal scales (Hoor et al., 2010; Bethet et al., 2007; Prather et al. 2011).

Transport of trace gases in CTMs is determined by several factors, for which various choices are possible. First, winds and the choice of advection scheme determine the large scale dispersion of tracers. Second, parameterised sub-grid-scale processes like boundary layer mixing and convection determine vertical gradients and the rate of IH transport. Finally, other differences may be caused by the horizontal and vertical grid of the CTM, and other issues related to spatial and temporal integration. To investigate the impact of these choices in CTMs, this paper will present the first results of the TransCom age-of-air (AoA) intercomparison study. The concept age-of-air originates from statospheric studies (Hall and Plumb, 1994; Neu and Plumb, 1999, Hall et al., 1999). In brief, the age spectrum in the stratosphere $G(x, t|t_0)$ is calculated as a type of Green function that propagates a tropospheric mixing ratio boundary condition into the stratosphere. Given a location x in the stratosphere, $G\delta t$ represents the fraction of air at x that was last in the troposphere a time $t - t_0$ to $t - t_0 + \delta t$ ago (Hall et al., 1999). In practical model applications focussing on stratospheric age spectra, $G(x, t|t_0)$ is calculated as the response of a time-dependent boundary condition $\delta(t - t_0)$ specified in a forcing volume in the troposphere. More recently, this concept has also been applied to trospopheric studies (Holzer and Hall, 2000; Waugh et al., 2013; Holzer and Waugh, 2015). In this AoA intercomparion, we will only analyse the mean age of air. This property can be easily extracted from model simulations with linearly growing boundary conditions in a specified atmospheric volume. We will outline the intercomparison protocol to in section 2. The resulting model output focussing on the simulation period 1988-2014 of 6 CTMs is compared in section 3, and discussed in section 4. Finally, the main conclusions are summarized in section 5.

1.3 2 Method

In order to compare transport time scales of a suite of CTMs, a protocol was developed that allows a straightforward implementation in existing atmospheric models. We defined seven AoA) tracers (Table 1) for which linearly growing boundary conditions are applied. All tracers are initialized with zero initial conditions at 1-1-1988, and modellers were requested to simulate up to 1-1-2015.

Table 1: The seven AoA tracers and their focring volume

AoA Tracer	Forcing volume
Surface	Surface < 100 m
NHsurface	NH surface < 100 m
SHsurface	SH surface < 100 m
Land	Land < 100 m
Ocean	Ocean < 100 m
Troposphere	Troposphere
Stratosphere	Stratosphere

For practical reasons the division between troposphere and stratosphere is defined as the statical pressure surface (in Pa), given by Lawrence et al. (2011):

$$P_{tropopause} = 3.00 \times 10^4 - 2.15 \times 10^4 (\cos(lat))^2 \quad (1)$$

This pressure surface thus varies between 300 hPa at the poles to 85 hPa at the equator. Note that this definition ignores dynamical and seasonal variations in the tropopause.

According to the protocol, the mixing ratio in the forcing volume is set every time step to a value $B = f \times t$, with t the elapsed time (in s) since 1-1-1988, and f a forcing constant of $1 \times 10^{-15} \mathrm{s}^{-1}$. As a result, the mixing ratio in the forcing volume will have a value of 852.0768 nmol mol^{-1} at the end of the simulation, and lower elsewhere. In theory, numerical issues with advection might lead to small wiggles in the vicinity of strong mixing ratio gradients. This may result in small unphysical negative mixing ratios that cannot be handled by some CTMs. To remedy this, models may be initialized with a uniform 100 nmol mol^{-1} initial condition, a value that is subtracted before further analysis.

Modellers are requested to calculate the exact fraction of the gridbox within the forcing volume. For the surface tracers, this calculation involves the land mask, the fraction of the grix box on either the NH and SH, and the geopotential height. For the stratosphere and troposphere tracer, the fraction of the box in either the troposphere or stratosphere needs to be evaluated. The protocol provides example code to help with the implementation. Importantly, the mixing ratio of the gridboxes within the forcing volume should be set according to:

$$X_{new} = f_{set} \times B + (1 - f_{set}) \times X_{old} \quad (2)$$

where f_{set} is the fraction of the grixbox within the forcing volume, and X_{old} the mixing ratio before the forcing procedure. Note that in locations where $f_{set} = 0$, nothing needs to be changed, and the mixing ratio changes are purely driven by transport from the forcing volume. To diagnose AoA, the simulated mixing ratios X in the atmosphere can be converted into AoA by $L = t - \frac{X}{f}$, with L the AoA in seconds and t the elapsed time of the simulation.

Figure 1 shows the simulated mixing ratios for the tracer "Surface" along the Cabauw tower from May 6 to May 15, 2010, together with the derived AoA. We use here output from the TM5 model on 1×1 degree resolution (see Table 4). At 20 m above the surface during night-time AoA is generally close to zero, due to the fact that the volume is forced in the lowest 100 m, and vertical mixing is limited in a stable nocturnal boundary layer.

During daytime, however, older air from aloft is mixed in, and the AoA increases depending on the depth of the mixing layer and the strength of the vertical mixing. At 200 m, outside the forcing volume, air is generally older. In some nights, e.g. from May 8 to May 9, the surface gets decoupled from the airmasses aloft, signalling a stable boundary layer. Note that the depth of the lowest model layer is approximately 20 m, wich implies that this layer is entirely within the forcing volume. However, TM5 still calculates a non-zero AoA in the lowest model layer, because the mixing ratios are sampled after vertical transport, which mixes in older air (Krol et al., 2005). We do not provide recommendations on the sampling strategy, so other models may behave different in this respect. The current paper will focus on large scale transport timescales and we expect no major influence of this sampling strategy on the results.

```
In [2]: aoa.figure_cbw()
```

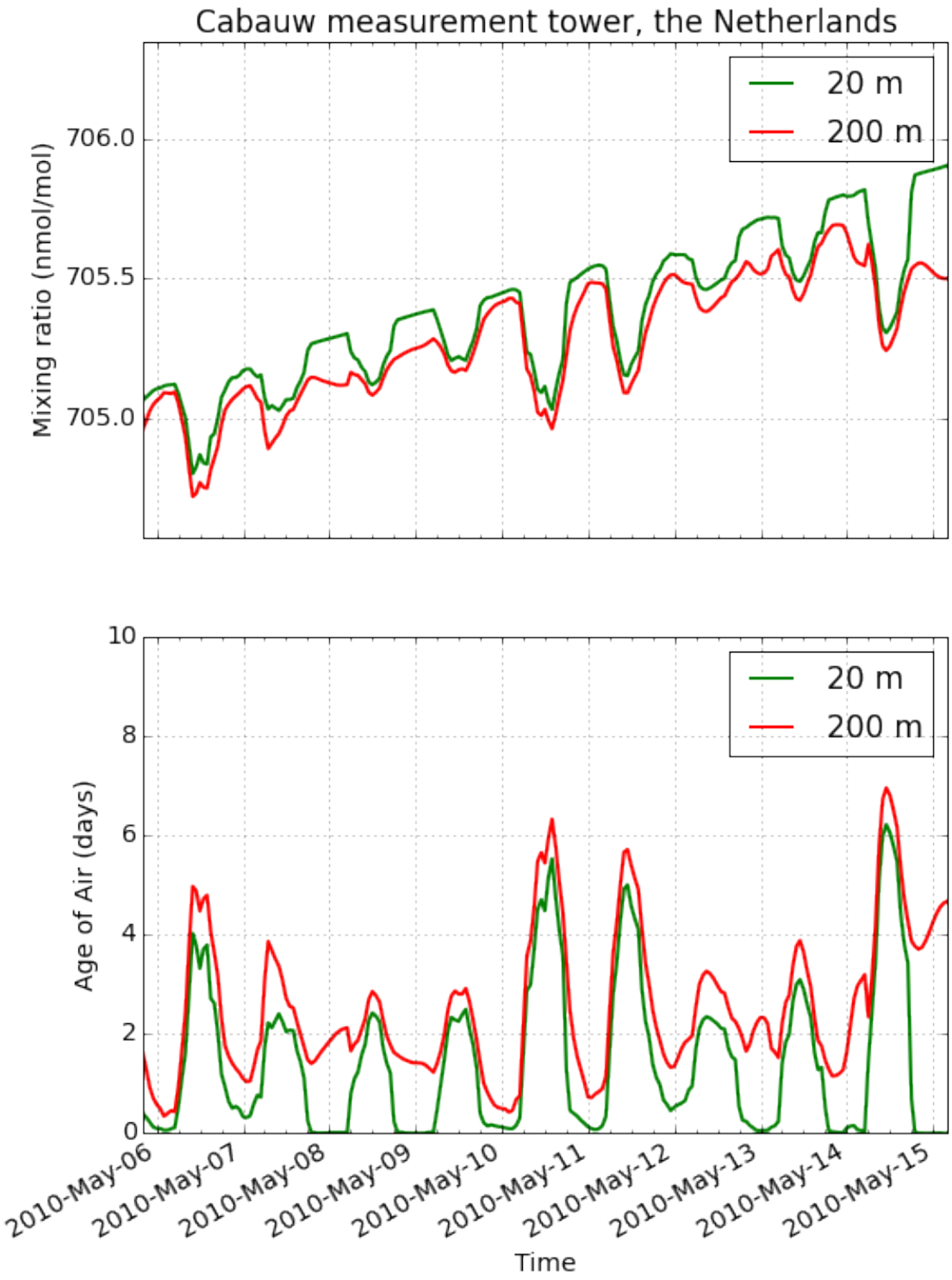

Figure 1: Upper panel: Simulated mixing ratios of an AoA tracer forced at the surface along the Cabauw measurement tower in the Netherlands during May 2010. Lower panel: Similar, but transferred into Age of Air.

To complement the AoA tracers, modellers are also requested to simulate the tracers listed in Table 2. Simulations of ^{222}Rn are intended to study vertical and synoptic scale transport (Jacob et al., 1997); SF_6 is used to diagnose IH transport, stratosphere-troposphere exchange, and stratospheric AoA; E90 is used to compare to Prather et al. (2011).

Table 2: Additional tracers

Homogeneous surface emissions (in kg m^{-2} s^{-1}) of E90 are calculated such that the mean steady-state atmospheric mixing ratio of E90 will approach 100 ppb:

$$E_{E90} = \frac{M_{atm} \times 100 \times 10^{-9}}{\tau_{E90} \times 4\pi r^2} \tag{3}$$

with M_{atm} the atmospheric mass [kg], r the radius of the Earth [m], and τ_{E90} the e-folding lifetime (90 days in units s) of E90.

Emissions of SF_6 based on EDGAR4.0 with corrections suggested by Levin et al. (2010) are given in Table 3 and plotted in Figure 2. The emission distribution is similar to Patra et al. (2011).

Table 3: yearly emissions of SF_6 for the period 1988-2015

Year	Source (mmol s^{-1})	Year	Source (mmol s^{-1})
1988	934	2002	1223
1989	938	2003	1258
1990	1036	2004	1268
1991	1116	2005	1299
1992	1210	2006	1366
1993	1303	2007	1475
1994	1381	2008	1555
1995	1392	2009	1577
1996	1312	2010	1599
1997	1208	2011	1642
1998	1162	2012	1685
1999	1177	2013	1729
2000	1201	2014	1772
2001	1197	2015	1816

```
In [3]: aoa.figure_sf6()
```

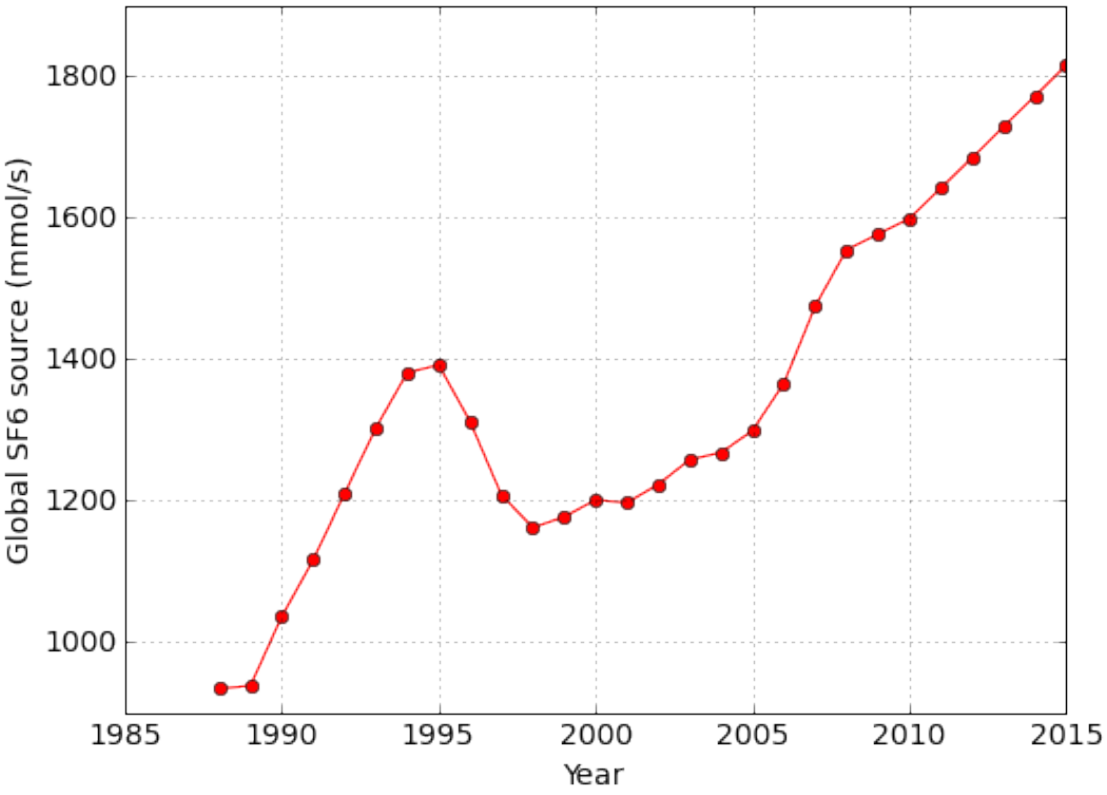

Figure 2: Yearly SF_6 emissions against emission year

Netcdf input files are provided with emissions on 1×1 degree resolution and initial SF_6 mixing ratios for 1-1-1988. In terms of output, modellers are requested to provide monthly mean mixing ratios and hourly mixing ratio time series at 247 atmospheric measurement stations. Furthermore, hourly atmospheric profiles of mixing ratios and meteorological variables (u-wind, v-wind, sureface pressure, boundary layer height, geopotential height) are requested at 119 locations. In this first analysis we will concentrate on the output of monthly mean mixing ratios that has been provided by 6 CTMs, some of them running in different configurations. Table 4 lists the participating models along with their horizontal and vertical resolution. For "off-line" models, the source of the meteorological data is also provided.

Table 4: Short-hand notation of the models participating in this study, along with model information

In the next sections, specific information on the participating models is given.

1.3.1 2.1 LMDZ

LMDz, developed at Laboratoire de Météorologie Dynamique with “z” stands for zoom capacity, is the global general circulation model of the IPSL Earth system model (Hourdin et al., 2006, 2013). Here, we include two versions of LMDz - LMDZ3 and LMDZ5A, both

with a horizontal resolution of 1.875° (latitude) × 3.75° (longitude) and a vertical resolution of 39 hybrid sigma-pressure levels, commonly chosen for global inverse studies using LMDz (Chevallier, 2015; Locatelli et al., 2015b; Yin et al., 2017). These two versions are different in terms of physical parameterization of deep convection and boundary layer mixing. LMDZ3 uses the deep convection scheme of Tiedtke (1989) and the boundary layer mixing scheme of Louis (1979). LMDZ5A is an updated version that uses the deep convection scheme of Emanuel (1991) and the boundary layer mixing parameterization from Deardorff (1966). More details regarding the configurations of the physics and comparison to other versions are described in Locatelli et al. (2015a). Sea surface temperature and sea ice coverage from the ERA-Interim climate reanalysis (Dee et al., 2011) produced by the European Centre for Medium-Range Weather Forecasts (ECMWF) are used as boundary conditions. Horizontal winds are nudged towards the ERA-Interim wind fields with a relaxation time of 3 hours.

1.3.2 2.2 TM5

The TM5 model (Krol et al., 2005) has different application areas with a common core. TM5 allows for a flexible grid definition with two-way nested zoom regions. This version is mainly used in inverse modelling applications, focussing on CO_2 (Peters et al., 2010), CH_4 (Houweling et al., 2014; Bergamaschi et al., 2013), and CO (Krol et al., 2013). The chemistry version of TM5 (Huijnen et al., 2010) was recently adopted for massive parallel computing (Williams et al., 2017). The AoA simulations were conducted in this so-called TM5-MP version.

Like earlier model versions, TM5-MP is driven using the ERA-Interim meteorological re-analysis (Dee et al., 2011) and updated every 3 h, with time-interpolation during time integration. For this intercomparison we include all 60 vertical levels provided by the ECMWF ERA-Interim reanalysis. Convective mass fluxes are derived from entrainment and detrainment rates from the ERA-Interim dataset. This replaces the convective parameterization use in the previous Transcom intercomparison (Patra et al., 2011), which was based on Tiedtke (1989). Recent analysis (Tsuruta, 2016) shows that the mass fluxes produced with the Gregory et al. (2000) convective scheme that forms the basis for the ERA-interim data set (Dee et al., 2011), lead to faster interhemispheric transport compared to the old model version using the Tiedtke (1989) scheme that was used in Patra et al. (2011).

The vertical diffusion in the free troposphere is calculated according to Louis (1979), and in the boundary layer by the approach of Holtslag and Boville (1993). Diurnal variability in the boundary layer height is determined using the parameterization of Vogelezang and Holtslag (1996). Advective fluxes are calculated using the slopes scheme (Russel and Lerner, 1981), with a refinement in time step whenever the Courant–Friedrichs–Lewy (CFL) criterion is violated.

The TM5 model is used in two versions that only differ in horizontal resolution. The version names TM5 3x2 simulated the AoA experiment at a resolution of 3° × 2° (longitude × latitude). In the version TM5 1x1 a horizontal resolution of 1° × 1° was used.

1.3.3 2.3 EMAC

The EMAC (ECHAM/MESSy Atmospheric Chemistry) model employed in this study, combines an updated version 2.50 of the MESSy (Modular Earth Submodel System) framework (Jöckel et al., 2005, 2010) with version 5.3.02 of the ECHAM5 (European Centre Hamburg) general circulation model (Roeckner et al., 2006). Our version of the EMAC model, first described by Jöckel et al. (2006), incorporates a recent update to convective transport of tracers (Ouwersloot et al., 2015) and is further improved upon to facilitate nudging of tracers according to Table 1. These modifications are included in version 2.52 of MESSy.

Dynamical properties are simulated by EMAC itself, but surface temperature, sea surface temperature, and flow divergence and vorticity are nudged towards ERA-Interim data. Convective mass fluxes are diagnosed in the CONVECT submodel (Tost et al., 2006), while the resulting transport is calculated by the CVTRANS model (Tost et al., 2010; Ouwersloot et al., 2015). The simulations with EMAC make use of 90 vertical hybrid sigma pressure levels. Data is available for two horizontal resolutions: T63 (192×96 grid) with a fixed time step of 6 min, and T106 (320×160 grid) with a fixed time step of 4 min.

1.3.4 2.4 ACTM

The CCSR/NIES/FRCGC (Center for Climate System Research/National Institute for Environmental Studies/Frontier Research Center for Global Change) atmospheric general circulation model (AGCM)-based chemistry-transport model (ACTM) is developed for simulations of long-lived gases in the atmosphere (Numaguti et al., 1997; Patra et al., 2009; 2014). The ACTM simulations are performed at a horizontal resolution of T42 spectral truncation (~2.8 x 2.8 deg) with 67 sigma levels in the vertical and model top at ~90 km. The horizontal winds and temperature of ACTM are nudged with Japan Meteorological Agency Reanalysis (JRA) data products (Onogi et al., 2007). The nudging forces the AGCM-derived meteorology towards the reanalyzed horizontal winds (U and V components) and temperature (T) with relaxation times of 1 and 2 days, respectively (except the top and bottom model layers).

To compute the heat and moisture exchange fluxes at the earth's surface, the AGCM is also supplied with interannually varying monthly-mean sea ice and sea-surface temperature (SST) fields from the Met Office Hadley Centre observational datasets (Rayner et al., 2003). Advective transport of moisture and tracers is obtained from a 4th order flux-form advection scheme using a monotonic Piecewise Parabolic Method (PPM) (Colella and Woodward, 1984) and a flux-form semi-Lagrangian scheme (Lin and Rood, 1996). Mass fluxes around the polar caps are calculated with a semi-Lagrangian scheme in polar stereo projection.

Subgrid-scale vertical fluxes of heat, moisture, and tracers are approximated using a non-local closure scheme based on Holtslag and Boville (1993) used in conjugation with the level 2 scheme of Mellor and Yamada (1974). The cumulus parameterization scheme is based on Arakawa and Schubert (1974) with some simplifications described in Numaguti et al. (1997). The updraft and downdraft of tracers by cumulus convection are calculated

by using the cloud mass flux estimated in the cumulus parameterization scheme.

1.3.5 2.5 NIES

The National Institute for Environmental Studies (NIES) Eulerian three-dimensional offline transport model is driven by the Japanese Meteorological Agency Climate Data Assimilation System (JCDAS) datasets (Onogi et al., 2007). It employs a reduced horizontal latitude–longitude grid with a spatial resolution of 2.5° × 2.5° near the equator (Belikov et al., 2011) and a flexible hybrid sigma–isentropic (σ–θ) vertical coordinate, which includes 32 levels from the surface up to 5 hPa (Belikov et al., 2013a). The parametrization of turbulent diffusivity separates transport processes in the planetary boundary layer (provided by the ECMWF ERA-Interim reanalysis) from the free troposphere following the approach by Hack et al. (1993). Vertcal mass fluxes related to cumulus convection are computed using conservation equations of moisture and are based on the distribution of convective precipitation in a cumulus cell, which is provided by the reanalysis dataset (Kuo, 1965; Belikov et al., 2013b). This modified Kuo-type parameterization scheme for convective updrafts and downdrafts includes entrainment and detrainment processes.

1.3.6 2.6 TOMCAT

TOMCAT/SLIMCAT is a global 3-D off-line chemical transport model (Chipperfield, 2006). It is used to study a range of chemistry-aerosol-transport issues in the troposphere (e.g. Monks et al., 2012) and stratosphere (e.g. Chipperfield et al., 2015). The model is usually forced by ECMWF meteorological (re)analyses, although GCM output can also be used. When using ECMWF fields, as in the experiments described here, the model reads in the 6-hourly fields of temperature, humidity, vorticity, divergence and surface pressure. The resolved vertical motion is calculated online from the vorticity. The model has different options for the parameterisations of sub-gridscale tracer transport by convection (Stockwell and Chipperfield, 1999; Feng et al., 2011) and boundary layer mixing (Louis, 1979; Holtslag and Boville, 1993). Tracer advection is performed using the conservation of second-order moments scheme of Prather (1986). For the experiments the model was run at horizontal resolution of 2.8° × 2.8° with 60 hybrid sigma-pressure levels from the surface to ~60 km. The model was forced by ECMWF ERA-Interim reanalyses. Convective mass fluxes were diagnosed online using a version of the Tiedtke scheme (Stockwell and Chipperfield, 1999) and mixing in the boundary layer is based on the local scheme of Louis (1979).

1.4 3 Results

1.4.1 3.1 Tropospheric AoA

First, we focus on zonal averages to investigate differences among the models in IH and vertical transport in the troposphere. Monthly mean mixing ratios (and pressure fields) of the participating models have been averaged zonally, and converted to AoA. Contour

plots of these latitude-pressure arrays are presented in figures 3, 4, and 5 for the AoA tracers Surface, NHsurface, and SHsurface, respectively (see table 1).

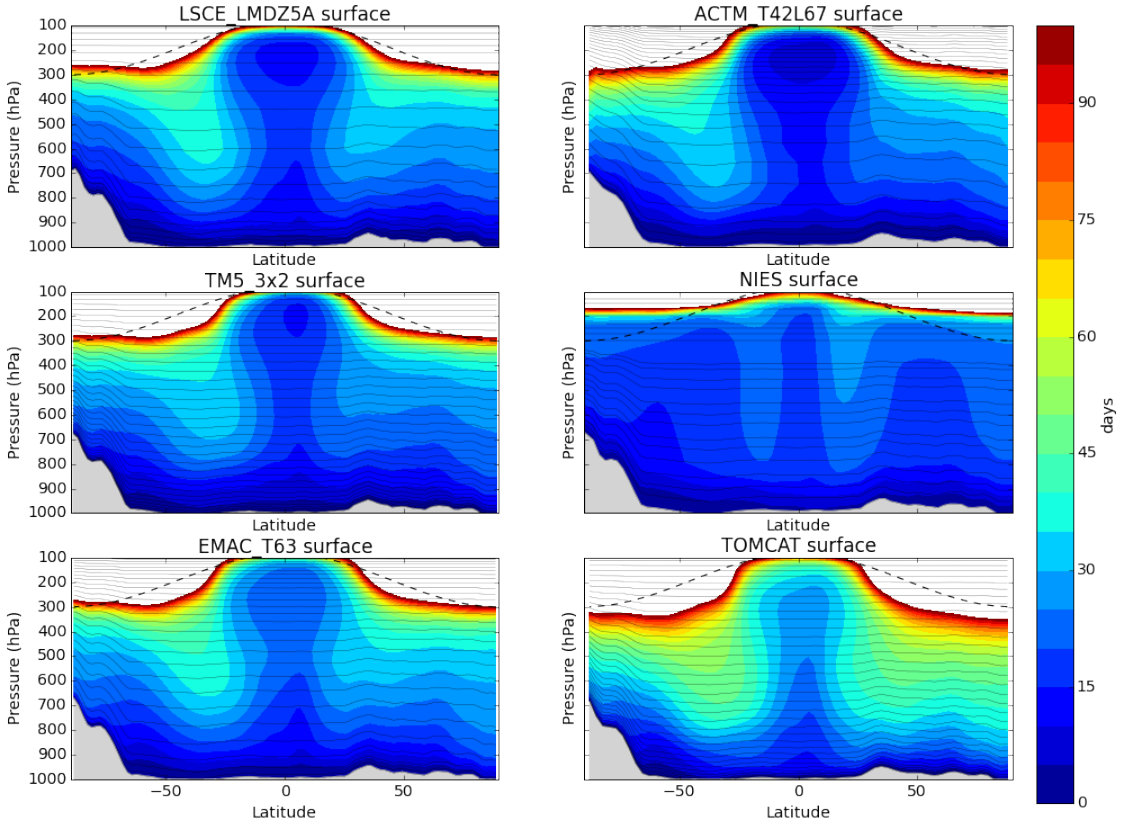

Figure 3: Zonally averaged AoA in the troposphere for the tracer "Surface". The results have been averaged over the period 2000-2010 (11 years). The light grey areas correspond to the zonal mean orography in the models. The thin black lines denote the mid-pressure levels of the models. The dotted black line denotes the climatological tropopause. The white areas correspond to areas in which the air is older than 100 days.

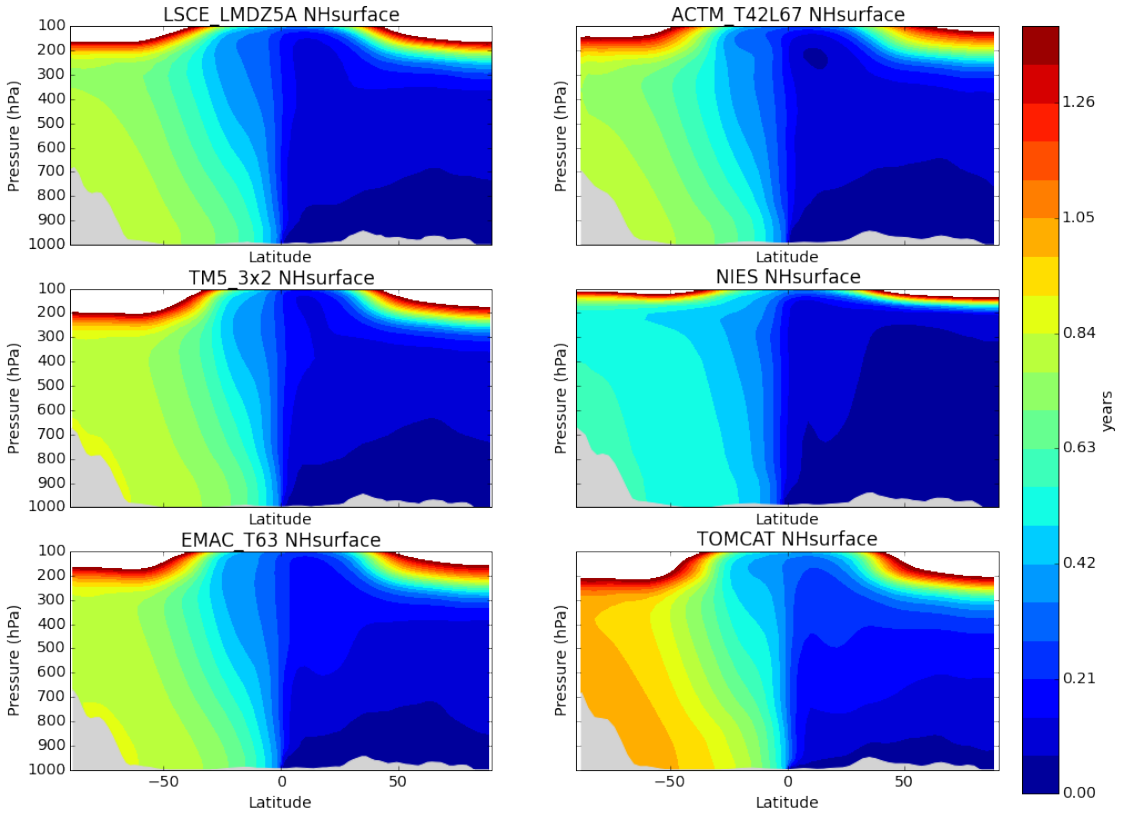

Figure 4: Zonally averaged AoA in the troposphere for the tracer "NHsurface". The results have been averaged over the period 2000-2010 (11 years). The light grey areas correspond to the zonal mean orography in the models. The white areas correspond to regions in which the air is older than 1.4 years.

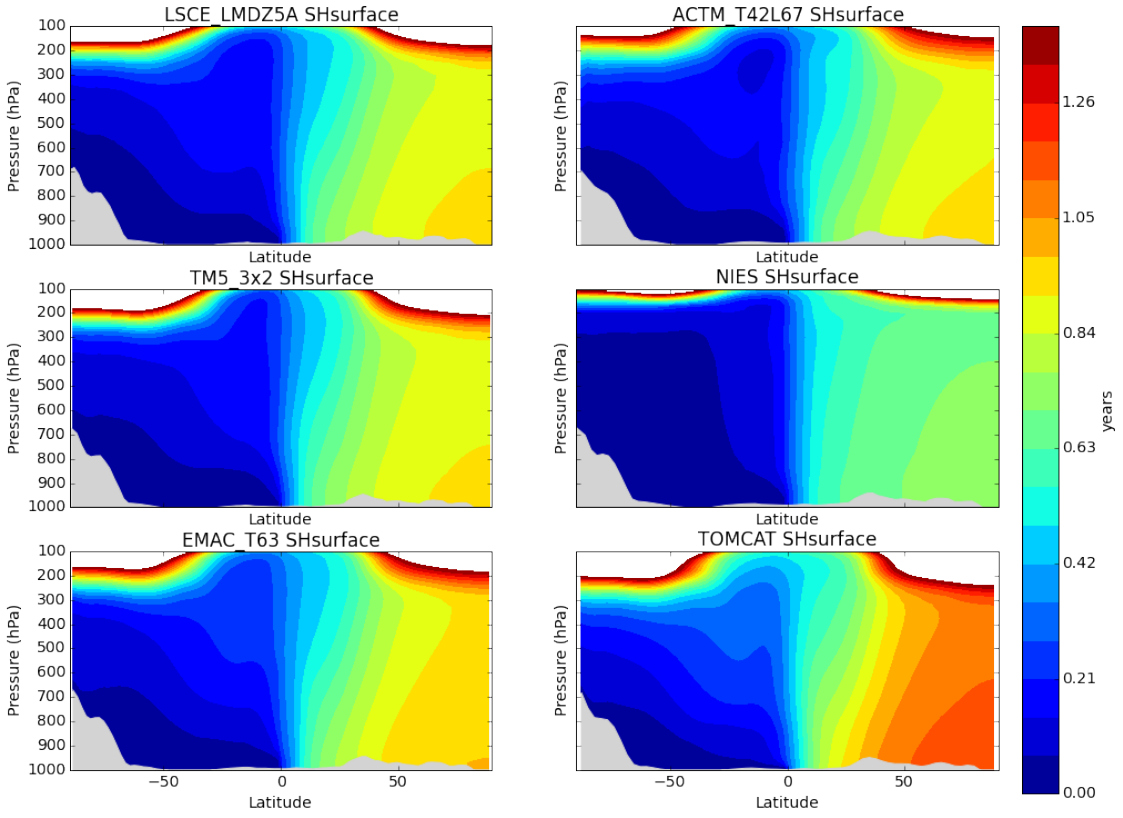

Figure 5: Zonally averaged AoA in the troposphere for the tracer "SHsurface". The results have been averaged over the period 2000-2010 (11 years). The light grey areas correspond to the zonal mean orography in the models. The white areas correspond to regions in which the air is older than 1.4 years.

The AoA in the troposphere derived from the "Surface" tracer is generally younger than 100 days (figure 3). The 100 day contour sharply marks the transition to the stratosphere at around 300 hPa at the poles. In the tropics this transition is located at a pressure smaller than 100 hPa. This generally agrees with the definition of the climatological tropopause given by Lawrence et al. (2001) and which is also used in the AoA protocol (see Section 2). Deep convective transport drives the vertical transport in the tropics, and this deep convective region is bounded by tongues of older air connected to the stratosphere, signalling stratosphere-troposphere exchange. Although all models agree on this general pattern, clear differences are also present. Deep convective mixing in the tropics is strongest in ACTM and NIES, while TOMCAT generally shows slower vertical mixing and larger AoA gradients between the surface and the upper troposphere. In NIES, convection leads to deep mixing also outside the tropical latitudes. This leads to an elevated tropopause compared to other models.

The tracers "NHsurface" and "SHsurface" are used to diagnose IH transport. Generally, the air at the poles has an age between 0.6 and 1.2 years. Here, all models agree on an interesting asymmetry: AoA derived from "SHsurface" around the North Pole is older than AoA derived from "NHsurface" around the South Pole. ACTM and NIES, which

were diagnosed with fast vertical mixing, show generally young air around the poles, while TOMCAT (with slow vertical mixing) has old air around the poles. Figures 4 and 5 illustrate that exchange of air between the hemispheres proceeds faster at higher altitudes (200-300 hPa), and consequently steep AoA gradients are observed close to the surface in the tropics.

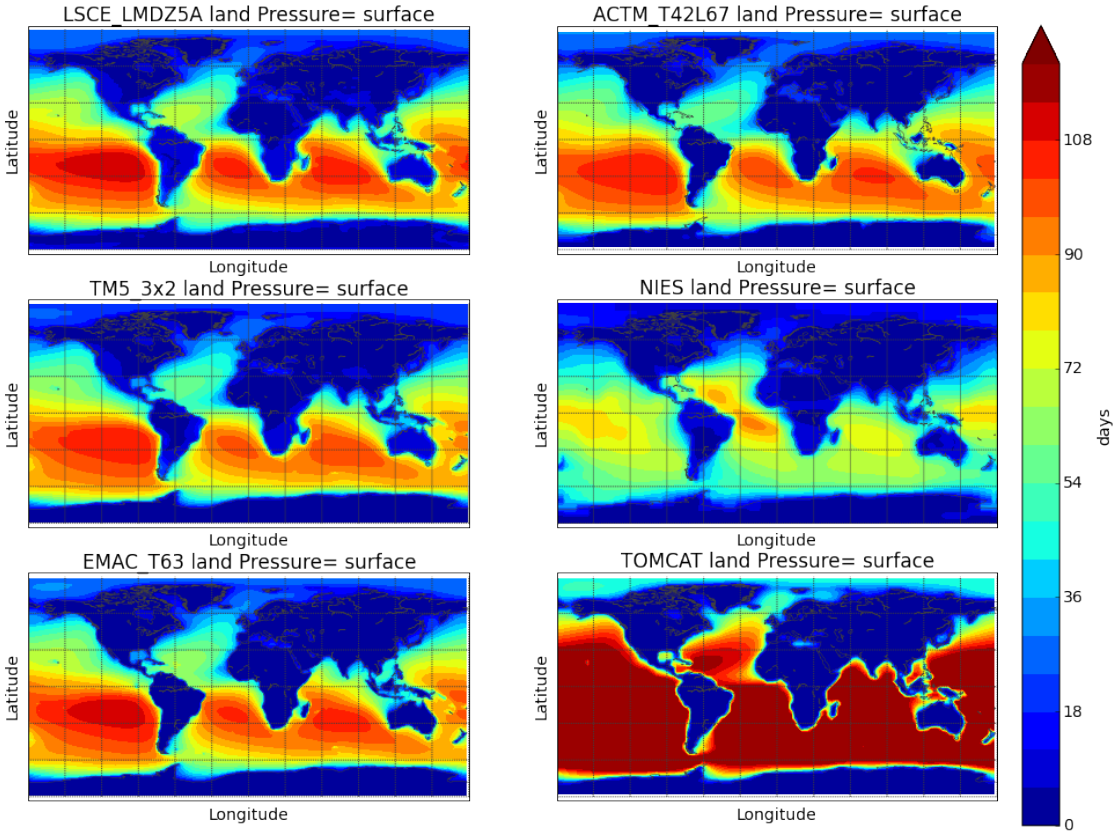

Figure 6: Latitude-longitude plot of the AoA derived from the "Land" tracer evaluated in the lowest model layer. The results have been averaged over the period 2000-2010 (11 years). Ages older than 120 days appear in dark red.

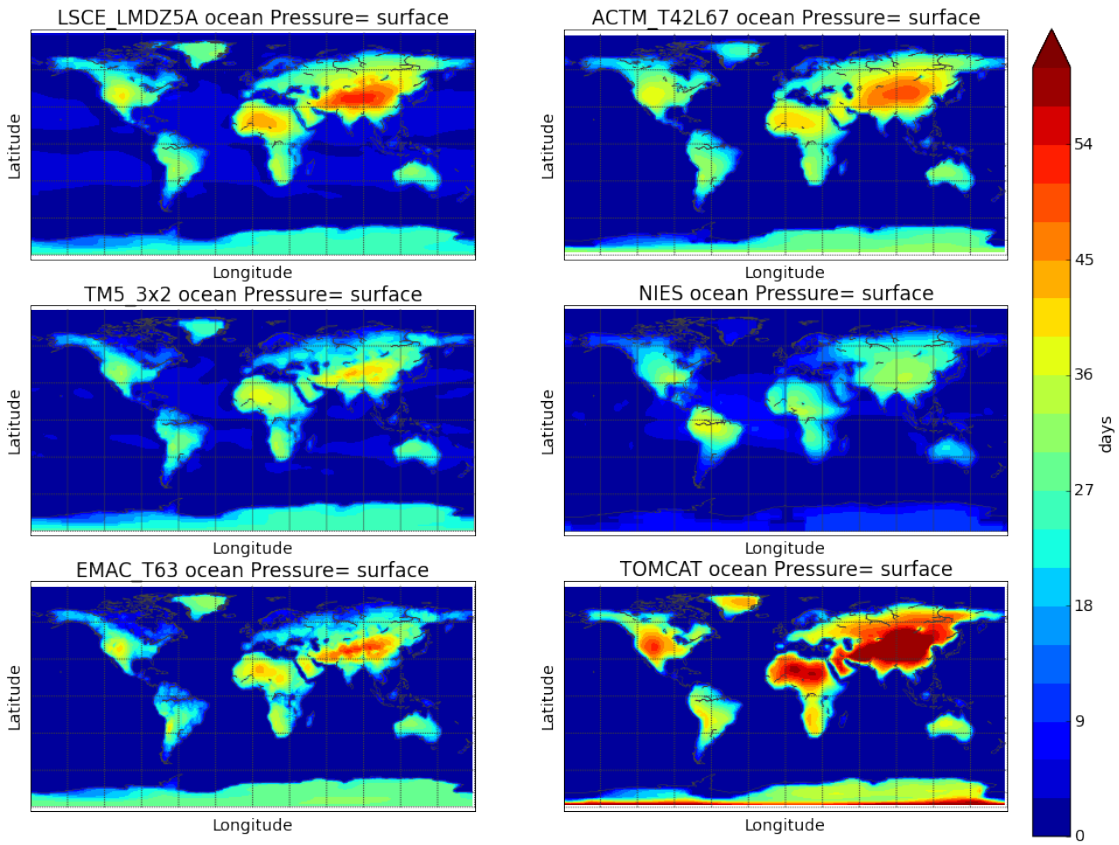

Figure 7: Latitude-longitude plot of the AoA derived from the "Ocean" tracer evaluated in the lowest model layer. The results have been averaged over the period 2000-2010 (11 years). Ages older than 60 days appear in dark red.

1.4.2 3.2 AoA derived from "Land" and "Ocean" tracers

Figures 6 and 7 show AoA derived from the "Land" and "Ocean" tracer, respectively, evaluated in the lowest model level. Oldest air related to "last contact with land" is found over the Southern Oceans, with ages older than 100 days (except for NIES). Models generally agree on the fact that old air is found in the stationary high pressure areas over the ocean that are related to the Hadley and Walker circulations. The TOMCAT model has systemetically larger AoA. Dominant land-ocean transport patterns are easily discerned in figure 6. Young air over oceans is found south-east of South America, north-west of Australia, and towards the north-east of North-America and Asia, associated with the jet-stream.

The AoA derived from the "Ocean" tracer (figure 7) generally shows ages less than 60 days over land, with the older ages logically located in areas deep inland. Although these patterns are similar in all models, the spread is considerable, with TOMCAT showing the oldest air, and NIES and TM5 showing the youngest air over land surfaces. These differences are likely related to the boundary layer parameterizations in the models. This

vertical transport process mixes in oceanic air into the boundary layer over land. In general, young air over land is connected to dominant circulation patterns like the monsoon, trade winds, and jet-streams.

1.4.3 3.3 Stratospheric AoA

Since not all participating models used the recommended climatological division between stratosphere and troposphere, we use the "Surface" tracer to compare the simulated stratospheric AoA. Here it should be noted that the TOMCAT AoA is already systematically older at the tropopause. In Figure 8 the stratospheric AoA is plotted for all models from 100 hPa to the top of the atmosphere, averaged over the period 2000-2010 (11 years). As expected, oldest AoA is found at the high-altitude poles. Considerable model spread is found with the oldest air (up to 7 years) in LMDZ5A and the youngest air in ACTM and NIES. Also the width of the "tropical pipe" differs: LMDZ and ACTM show the broadest opwelling region in the tropics, in agreement with the tropospheric AoA in figure 3. The transport in EMAC, LMDZ, and TM5 are all driven by ERA-interim meteorology (see Table 4). Apparently, the AoA in the stratosphere is not only determined by the driving meteorological data, but also by the treatment of advection, nudging parameters, and the number of vertical layers in the model.

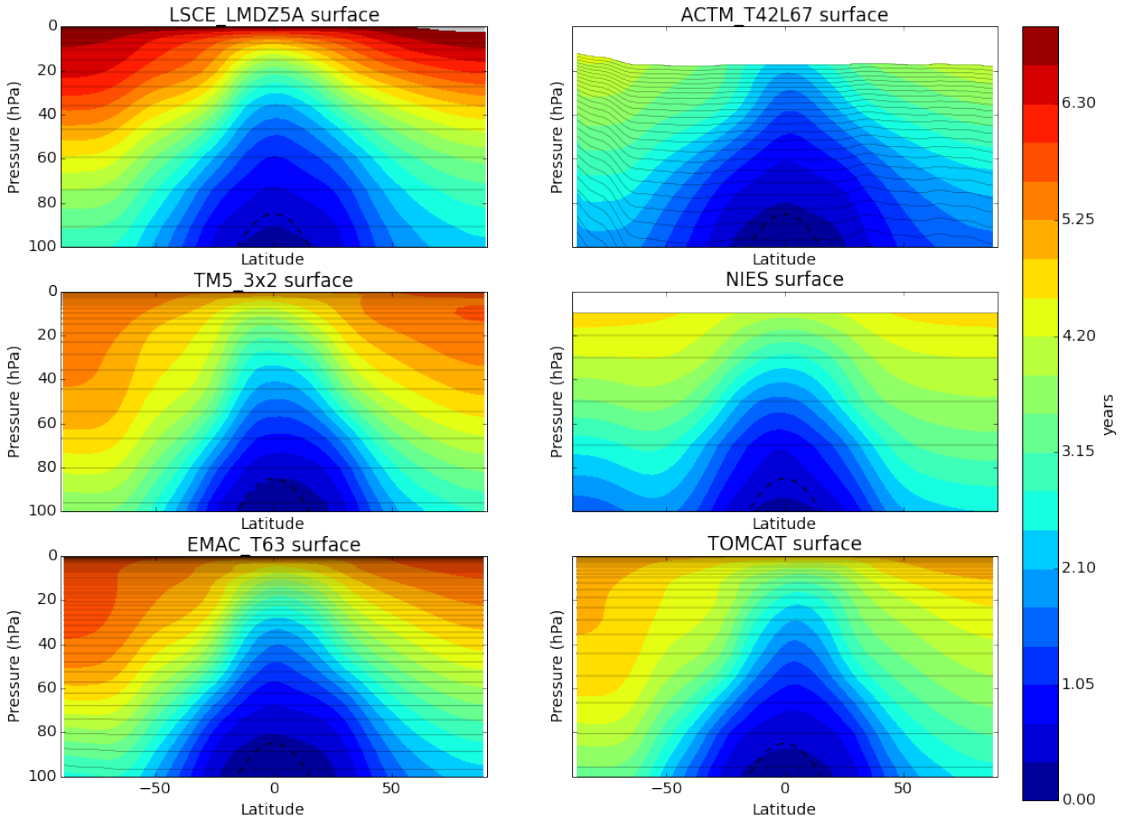

Figure 8: Zonally averaged AoA in the stratosphere for the tracer "Surface". The results have been averaged over the period 2000-2010 (11 years). The thin black lines denote the mid-pressure levels of the model. For the ACTM model, this level is at around 17 hPa for the upper layer. The dotted black line denotes the climatological tropopause.

1.4.4 3.4 Interhemispheric transport

In this section, we compare the interhemispheric transport times using tracers "NHsurface" and "SHsurface" to the simulated latitudional gradients of SF_6. To this end, we show in Figure 9 (upper panel) the simulated zonal average latitudional SF_6 gradient at the surface. All gradients have been scaled relative to the South Pole SF_6 mixing ratio. Shown for comparison are the latitudional gradients measured by the National Oceanic & Atmospheric Administration Earth System Research Labatory (NOAA/ESRL) (Hall et al., 2011). We use the combined data set constructed from flask data measured by the Halocarbons and other Atmospheric Trace Species (HATS) group and hourly CATS data (downloaded from https://www.esrl.noaa.gov/gmd/hats/combined/SF6.html), and include only stations with a full measurement record in the period 2000-2011. Subsequently, the difference with respect to the South Pole is calculated as an 11 year time series with monthly time resolution. The mean and standard deviations of these time series are added to the modeled latitudional gradients in figure 9. Since the selected model results are averages over all longitudes, including the land masses with high emissions, modeled zonal averages exceed the observations at NH mid-latitudes. Most notably, high altitude stations like Niwot Ridge (3523 masl) and Muana Loa (3397 masl) show much smaller concentration differences with respect to the South Pole than e.g. Cape Kumukahi at sea level. This is confirmed by the middle panel, in which the modeled SF_6 fields are zonally averaged over the clean Pacific Ocean only (from 150 E/W to the dateline). In this average all models except NIES agree well within 0.1 pmol mol^{-1} on the latitudional gradient. Due to too strong vertical mixing, the NIES model underestimates the latitudional SF_6 gradient. A more detailed analysis of the modeled SF_6 gradients is beyond the scope of the current paper, but modeled mixing ratios at station locations are available for most participating models.

The lower panel of figure 9 depicts a composite of the AoA of tracer "NHsurface" at the SH surface, and of tracer "SHsurface" at the NH surface. Again, all results are averages over 2000-2010 (11 years) and include all longitudes in the zonal average. The lower panel confirms the NH-SH asymmetry noted earlier in section 3.1, but also makes clear that the asymmetry differs per model. Figure 10 highlights the NH-SH asymmetry by subtracting the "NHsurface" AoA sampled at the SH surface from the "SHsurface" AoA sampled at the NH surface. In all models, differences grow gradually from 10° latitude to the pole, where the AoA differences range between 0.10 year (TM5_3x2) and 0.17 year (EMAC_T106, NIES). The higher model resolution versions (TM5_1x1, EMAC_T106) show larger AoA differences compared to the lower resolution versions.

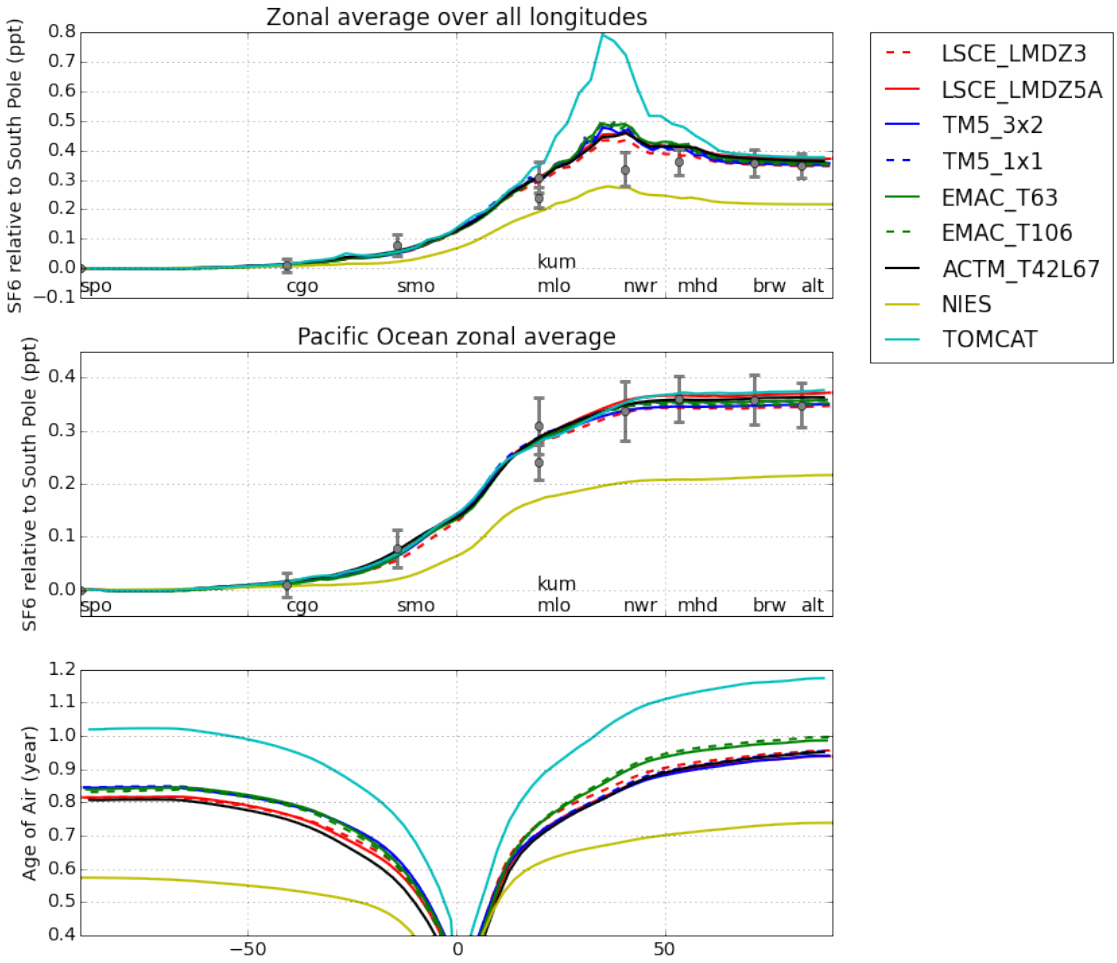

Figure 9: Upper two panels: Latitudional gradient of SF_6 (ppt) at the surface, averaged over 2000-2010 (11 years). The upper panel includes all longitudes in the modeled zonal average. The middle panel includes only llongitudes over the Pacific Ocean (150 W/E to the dateline) Modeled gradients have been scaled with respect to the South Pole. The grey symbols and errorbars are calculated from the combined dataset constructed from flask data measured by the Halocarbons and other Atmospheric Trace Species (HATS) group from NOAA/ESRL and hourly CATS data (https://www.esrl.noaa.gov/gmd/hats/combined/SF6.html). Three letter codes at the bottom refer to the stations (alt = Alert, Canada; brw = Pt. Barrow, Alaska, USA; nwr = Niwot Ridge, Colorado, USA; brw = Pt. Barrow, Alaska, USA; kum = Cape Kumukahi, Hawaii, USA; mlo = Mauna Loa, Hawaii, USA; smo = Cape Matatula, American Samoa; cgo = Cape Grim, Tasmania, Australia; spo = South Pole; mhd = Mace Head, Ireland). Errorbars are calculated as the standard deviation of monthly time series of the station data relative to the South Pole station. Lower panel: Composite of the AoA of the NHsurface tracer at the SH and the SHsurface tracer at the NH (see main text, averaged over 2000-2010).

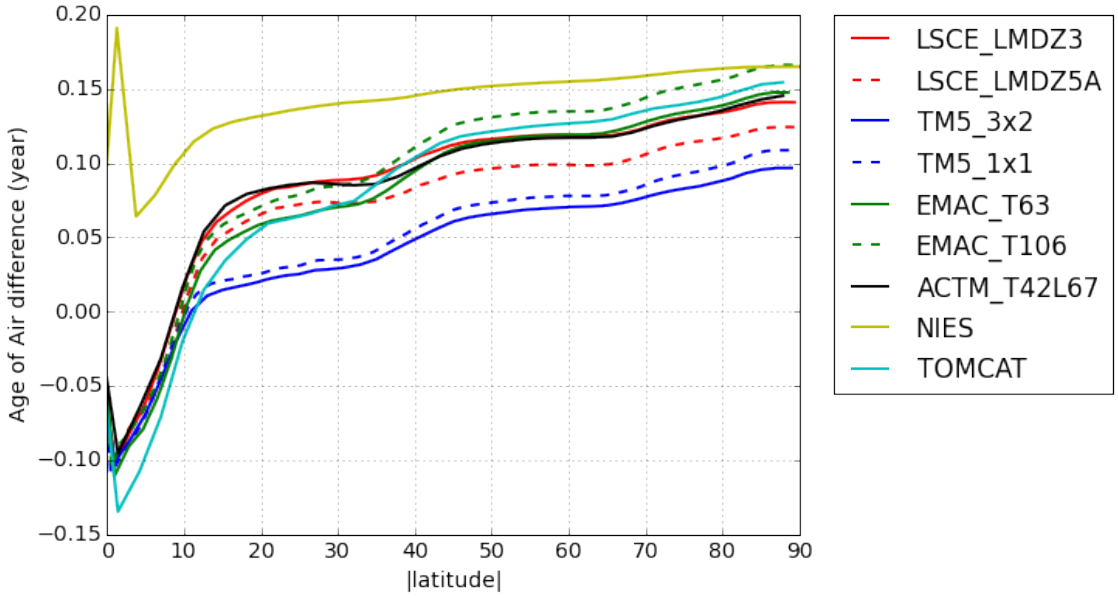

Figure 10: AoA difference calculated from the values in the lower panel of figure 9. The NHsurface AoA at the SH is subtracted from the SHsurface AOA at the NH, and plotted against latitude. AoA is evaluated at the surface and averaged over 2000-2010 (11 years).

From the figure 9 (upper and lower panel) it is clear that the TOMCAT model shows the strongest SF_6 gradient, along with the slowest IH transport as diagnosed from the tracers "NHsurface" and "SHsurface". NIES shows the opposite. Differences between the other models are less pronounced. The gradient of SF_6 is driven by emissions that take place mainly at midlatitude land masses on the NH. In contrast, the tracers "NHsurface" and "SHsurface" are forced at the entire surface of both hemispheres. To make a meaningfull comparison to the simulated latitudional gradients of SF_6, we evaluate the AoA of tracers "NHsurface" and "SHsurface" at respectively 40°S and 40°N, at the surface of the models. By adding these two ages, we align the resulting composite AoA with the bulk of the calculated latitudional SF_6 gradient between the South Pole and 40°N. The result is shown in Figure 11. Indeed, using this AoA metric, there appears a clear linair relation between the diagnosed AoA and the simulated SF_6 gradients. While the two versions of EMAC and TM5 show almost identical results, the LMDZ models differ more. This is likely related to the fact that the TM5 and EMAC model versions only differ in resolution, while in LMDZ the models differ in the parameterization of convection (see Section 2.1).

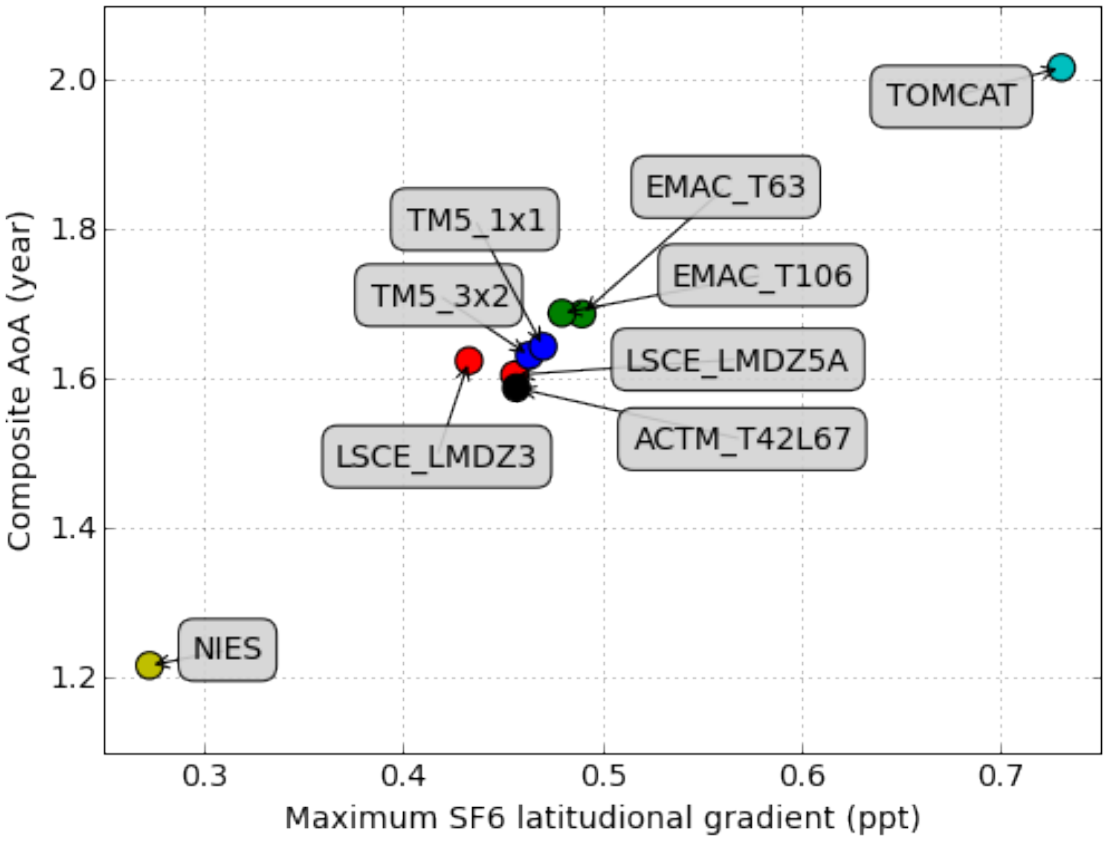

Figure 11: Composite AoA plotted against the modelled SF_6 gradient. The composite AoA is calculated as the sum of the 40^{o}N AoA of tracer SHsurface and the 40^{o}S AoA of tracer NHsurface. The maximum SF_6 gradient is taken as the maximum of the curves plotted in the upper panel of figure 9. Results are averaged over 2000-2010 (11 years).

1.4.5 3.5 Vertical transport

In this section, we compare the vertical transport in the tropospere, as diagnosed from the "land" tracer to the simulated vertical gradients of ^{222}Rn. To this end, we show in Figure 12 (left-hand panel) the simulated mean vertical profiles, area weighted between 60 °S and 60 °N on a log-scale. Clearly, the TOMCAT model retains the ^{222}Rn closer to the surface, because slower vertical mixing. The other models mix the ^{222}Rn to higher altitudes, but larger differences are found at pressures smaller than 400 hPa, where some models exhibit a more pronouced C-shape profile (e.g. ACTM, LMDZ5A). The right-hand panel of figure 12 shows the vertical profiles of the AoA of tracer "land", averaged in the same manner.

To investigate consistent differences in vertical mixing between teh models, Figure 13 compares the simulated vertical gradient in ^{222}Rn to the simulated AoA profiles of the "land" tracer. Because ^{222}Rn decays radio-actively with a half-life of 3.8 days, we convert the vertical gradient of ^{222}Rn mixing ratio as:

$$\Delta = \ln {}^{222}Rn(950\,\text{hPa}) - \ln {}^{222}Rn(500\,\text{hPa}), \tag{4}$$

where we do not sample directly at the surface to avoid differences in sampling strategies between models. Here we quantify the gradient with respect to the 500 hPa level. In Figure 13 we plot the AoA gradient between 500 hPa and 950 hPa agains Δ. Again, the results of the different models show a high degree of lineair correlation, indicating that models with efficient vertical mixing (e.g. TM5, ACTM, NIES) have small AoA differences between de boundary layer and 500 hPa along with a flatter ^{222}Rn profile. Interestingly, the TM5 and EMAC models show that a higher model resolution leads to faster vertical mixing, in contrast to the results found for IH transport. This is likely due to the fact that deep convective mixing is a sub-grid scale process that is less prone to numerical diffusion. The two model versions of LMDZ that differ by their convective parameterization show distinct differences in the vertical profiles.

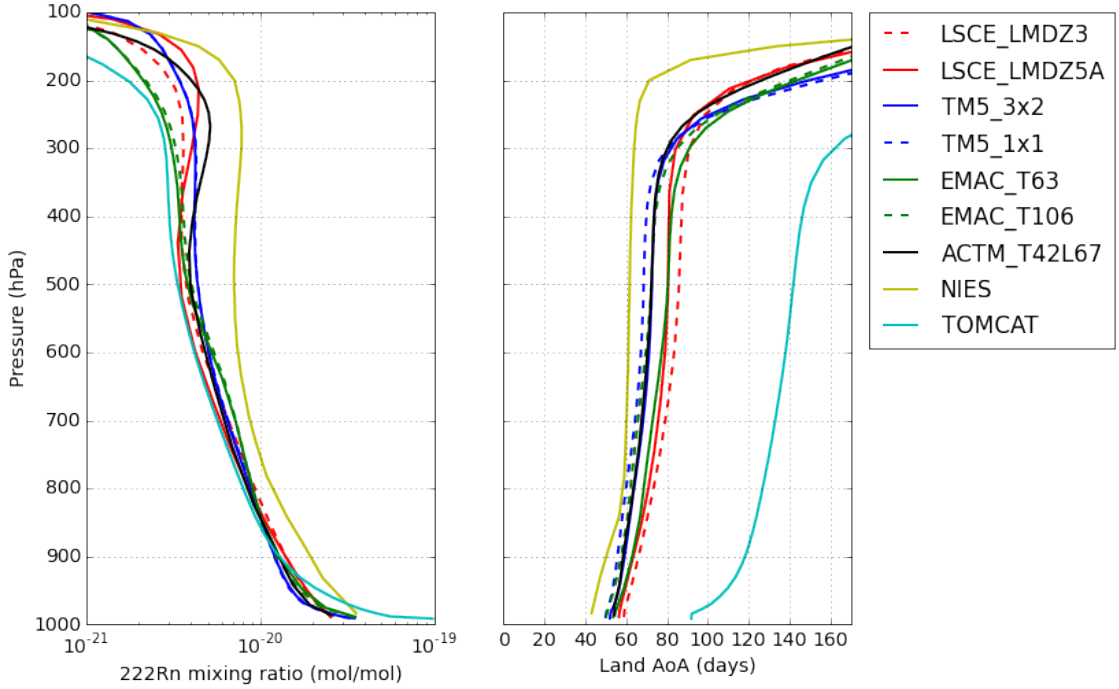

Figure 12: Vertical profiles of ^{222}Rn (left, logarithmic axis) and the AoA of the "land" tracer (right) simulated by the different models. The vertical profiles have been weighted-averaged between 60°N and 60°S and over the years 2000-2010 (11 years).

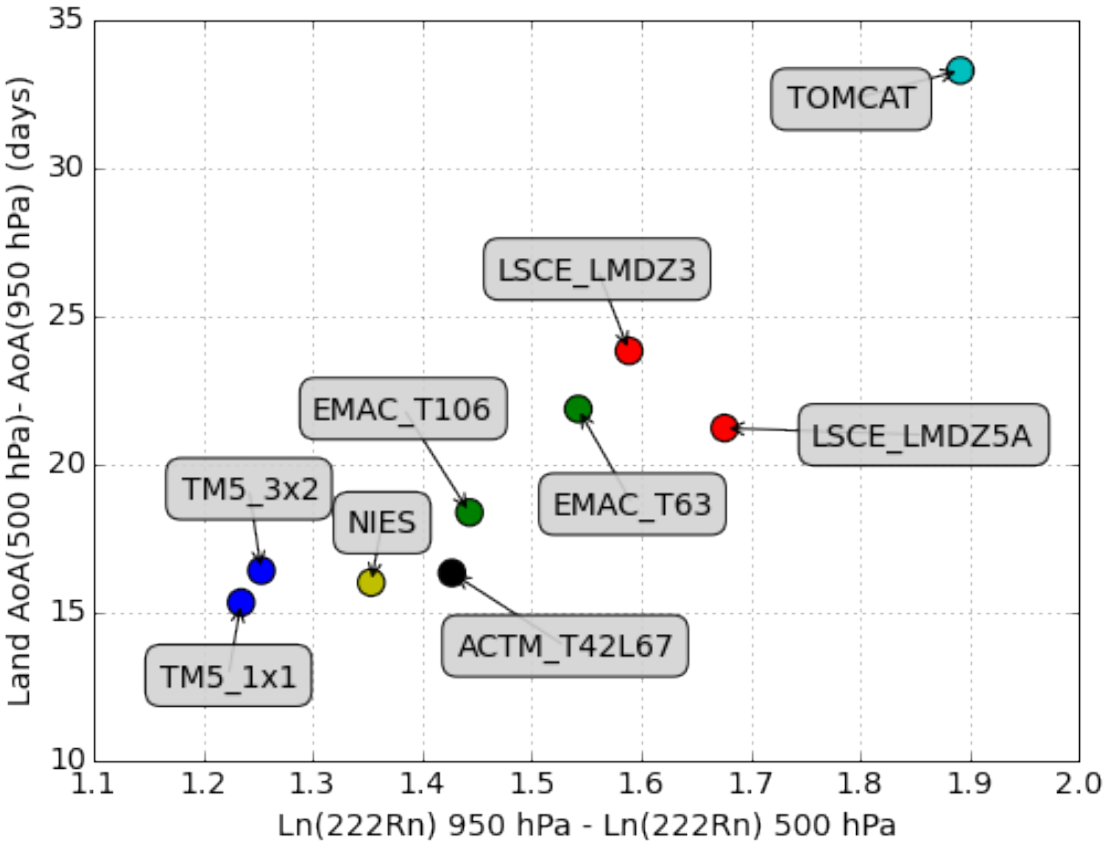

Figure 13: The 500 hPa - 950 hPa difference in AoA of the "land" tracer plotted against Δ: a measure for the vertical gradient in ^{222}Rn (see text). The vertical profiles used for the calculations are shown in figure 12.

1.4.6 3.6 Mapping the tropopause

Prather et al. (2011) introduced a tracer (E90) to delineate the boundary between troposphere and stratosphere in chemistry transport models. Driven by surface emissions and a decay rate of 90 days^{-1}, the E90 tracer is meant to quantify the rate of mixing of tropospheric air. The tropopause in the UCI CTM (Prather et al. (2011)) is defined as the isosurface on which the mixing ratio of E90 is 90 nmol mol^{-1}. Note that emissions of E90 are defined such that the global state state concentration of E90 is 100 nmol mol^{-1} (see section 2). Mixing ratios in the stratosphere are lower, due to the long transport times. As alternative for E90, the AoA tracer "Surface" may also be used to delineate the stratosphere from the troposphere, as shown in figure 3. In order to compare the tropopause pressure calculated by either E90 or the AoA surface tracer, we plot the tropopause pressure as a function of latitude in Figure 14. The tropoause pressure is calculated based on 2000-2010 zonal averages of E90 (unit nmol mol^{-1}) and "Surface" AoA (unit days). Per latitude the tropopause pressure is determined by interpolation to E90 = 90 nmol mol^{-1}

(dotted lines in figure 14) and to "Surface" AoA = 90 days (solid lines in figure 14). Results show a high level of consistency, although larger differences occur for several models. These difference are likely caused by the transport characteristics of the models. The "Surface" AoA simulation is forced by linearly increasing boundary conditions which are calculated back as AoA, while the E90 simulation is driven by surface emissions and a decay process with a 90 day turnover time. This causes different tracer gradients and hence difference in advective and convective transport. As a result, NIES and ACTM calculate systematically higher tropopause pressures for E90, while TM5 results are very similar for both tracers. When models are compared, both tracers calculate similar tropopause pressure differences, with NIES showing a very deep tropopause at higher latitudes and TOMCAT a shallower tropopause. Finally, all models, except for the NIES model, agree on a hemispheric asymmetric average tropopause with a tropopause pressure maximum around 55°S, likely associated with enhanced stratosphere–stratosphere exchange in the SH (Holton et al., 1995). In most models, this pressure maximum is more pronounced for the E90 tracer.

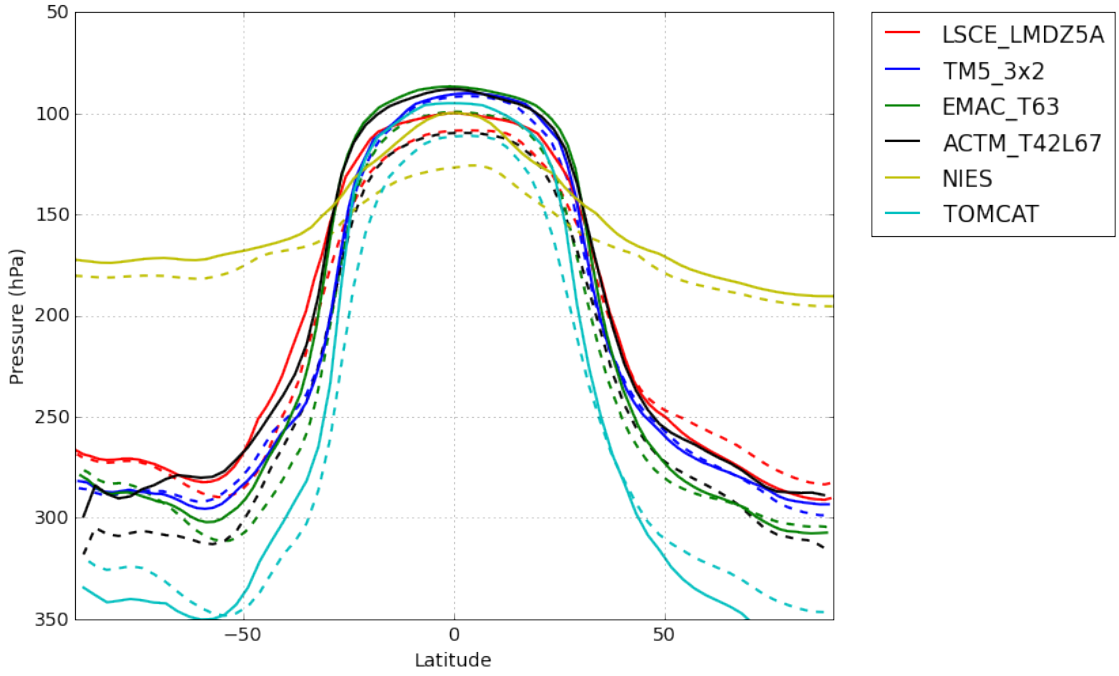

Figure 14: Zonal average tropopause pressure (average over 2000–2010) as a function of latitude, obtained from AoA tracer "surface" (solid lines) and E90 (dashed lines) for different models (see legend). Tropopause pressure is obtained from 1D lineair interpalation to 90 days for AoA tracer "surface" and to 90 nmol mol^{-1} for E90.

1.5 4 Discussion

This TRANSCOM AoA intercomparison shows that the tropospheric AoA concept provides useful information on model transport characteristics. It was shown that the IH

transport timescale in a particular model is strongly connected to the efficiency of vertical mixing and hence to the specific implementation of sub-grid-scale convective transport. The NIES model, which has very efficient convective mixing, shows fast IH mixing and a small IH SF_6 gradient. In contrast, the TOMCAT model shows weak vertical mixing and a stronger SF_6 gradient. The TM5 model, which was diagnosed with slow IH transport in the TRANSCOM methane intercomparison (Patra et al., 2011), now uses the Gregory convective fluxes stored in the ECMWF ERA-interim archive (Gregory et al., 2000; Tsuruta et al., 2016), which brings the OH transport times close to other models (see figure 11). This confirms that the implementation of sub-grid convective in CTMs deserves attention, specifically in atmospheric inversion studies. This is in line with the study of Stephens et al. (2007), which showed that the attribution of the global CO_2 land sink depends strongly on the vertical mixing in models.

We found an interesting hemispheric asymmetry in the IH transport times, with "older" NH air diagnosed with an AoA tracer forced at the SH surface, compared to the age of SH air, diagnosed with an AoA tracer forced at the NH surface. We attribute this to the effect of land-masses on the NH, which lead to an atmospheric stabilisation in winter, decoupling the boundary layer (BL) from the overlying free troposphere (FT). This is partly compensated by more effective mixing in summer, but the resulting net effect is well known as the "seasonal rectifier" (Denning et al., 1995). Thus, the AoA metric can also be used to quantify the strength of these rectifier effects in CTMs.

Another important timescale in CTMs is the mixing time of the BL and its coupling with the overlying FT. Together with the aforementioned "convection" timescale, these two quantities seem responsible for the main model diversity in this intercomparison. For instance, the TM5 model shows a relatively strong coupling between the BL and the FT, witnessed by (i) relatively young air of the ocean AoA tracer over land (figure 7), (ii) only a small IH difference in the AoA (figure 10), and (iii) a small 950 hPa – 500 hPa vertical gradient in ^{222}Rn and the land AoA tracer (figure 13). Differences with the EMAC, LMDZ, and ACTM models seem to be determined by the strenght of this BL-FT coupling. Differences of these models and NIES and TOMCAT seem to be driven by the convective parameterisation.

Other model differences, such as resolution, advection scheme, the meteorological driver data, and the vertical coordinate system may also play a role and may become more apparent on the smaller spatial and temporal scales that are not part of this first analysis. In mapping the tropopuase with either E90 or the AoA derived from the surface tracer (figure 14) model-dependent differences appeared that may be related to the treatment of atmospheric transport.

Our multi-model results agree qualitatively with the study of Waugh et al. (2013) that focused on SF_6 and a AoA tracer in a single model (GMI-MERRA). They found "older" AoA than derived from SF_6. The AoA simulations presented here allow for more detailed analyses in the future, including comparisons to earlier efforts to quantify tropospheric AoA based on observations (e.g. Holzer and Waugh (2015)).

The simple AoA concept exploited here is easily implemented in CTMs, and other modellers are encouraged to implement AoA tracers in their CTM. All model output, including analysis software is available for the scientific community for further analysis. The AoA protocol is also useful as benchmark for model development. Currently we are

coupling the TM5 model to the climate model EC-Earth (Hazeleger et al., 2010) and we hope to characterize changes in transport due to differences in driving meteorological data by using AoA. Finally, the analysis of the entire time series (1988-2015) might reveal trends in the Brewer Dobson circulation (Fu et al., 2015) or IH transport timescales.

1.6 Conclusions

This paper presents the first results of the TRANSOM AoA intercomparison with 6 participating models simulating 7 AoA tracers and 4 additional tracers over the time period 1988-2015. The main conclusions are:

- The IH transport time depends strongly on the strength of the convective parameterisation in the participating models. A strong correlation is found between derived IH transport times and SF_6 latitudional gradients
- IH transport proceeeds faster from the NH to the SH than from the SH to the NH. This is attributed to the seasonal rectifier effect
- BL mixing and venting to the FT over land varies among models, which leads to consistent differences in modeled vertical gradients
- The AoA concept can be used to map the tropopuase. At the tropopause the air has last been in contact with the surface 90 days ago (AoA = 90 days). For most models, the derived tropopuase pressure is in good agreement with the E90 tracer (Prather et al., 2011).
- Stratospheric AoA differs considerably among the participating models.

Model output, including analysis software is available for further analysis.

1.6.1 Acknowledgement

The TM5 model simulations and analysis was carried out on the Dutch national e-infrastructure with the support of SURF Cooperative. Paul Palmer is ackowledged for support of the initial Age of Air initiative.

1.6.2 References